Journal of the Korean Magnetic Resonance Society **2017**, *21*, 20-25
DOI 10.6564/JKMRS.2017.21.1.020

Backbone Assignment of Phosphorylated Cytoplasmic Domain B of Mannitol Transporter II^{Mtl} in *Thermoanaerobacter Tengcongensis*

Ko On Lee and Jeong-Yong Suh*

Department of Agricultural Biotechnology, Seoul National University, Seoul, 08826, Republic of Korea

Received Feb 01, 2017; Revised Feb 20, 2017; Accepted Mar 10, 2017

Abstract The cytoplasmic domains A and B of the mannitol transporter enzyme II^{Mtl} are covalently linked in *Escherichia coli*, but separately expressed in *Thermoanaerobacter Tengcongensis*. The phosphorylation of domain B (*Tt*IIB^{Mtl}) substantially increases the binding affinity to the domain A (*Tt*IIA^{Mtl}) in *T. Tengcongensis*. To understand the structural basis of the enhanced domain−domain interaction by protein phosphorylation, we obtained NMR backbone assignments of the phospho-*Tt*IIB^{Mtl} using a standard suite of triple resonance experiments. Our results will be useful to monitor chemical shift changes at the active site of phosphorylation and the binding interfaces.

Keywords backbone assignment, mannitol transporter Enzyme II, phosphorylated protein *Thermoanaerobacter Tengcongensis*

Introduction

The cytoplasmic phosphoryl transfer domains A and B of the mannitol transporter enzyme II^{Mtl} are covalently connected by a flexible peptide linker in mesophilic bacterium such as *Escherichia coli* (*Ec*),[1-3] whereas they are separately expressed in typical thermophilic bacterium, *Thermoanaerobacter Tengcongensis* (*Tt*).[4] Previous NMR studies have determined the three-dimensional structures of unphosphorylated *Ec*IIB^{Mtl} (PDB code : 1VRV)[5] and phosphorylated *Ec*IIB^{Mtl} (PDB code : 1VKR).[6] Both structures are composed of a central four beta strands, flanked by three alpha helices with identical global folds. However, there were small differences at the phosphorylation site where the phosphoryl group is engaged in multiple hydrogen bonds.[6] Further studies on their interaction and dynamics reported that the binding affinity between *Ec*IIA^{Mtl} and *Ec*IIB^{Mtl} was extremely weak (K_D = ~3.7 mM).[7] The flexible linker was important to confine the two domains within an effective distance of 46 Å, enabling a facile intramolecular domain association.[8,9]

*Tt*IIA^{Mtl} and *Tt*IIB^{Mtl} do not have a connecting linker that facilitates the association. Instead, *Tt*IIA^{Mtl} employs key interfacial residues to enhance the interaction with phosphorylated *Tt*IIB^{Mtl}.[10] Even though the structures were very similar, phospho-*Tt*IIB^{Mtl} (K_D = ~120 μM) showed 14 times stronger affinity than free *Tt*IIB^{Mtl} (K_D = ~1.7 mM).

To understand the differential binding according to the phosphorylation state, structural and dynamics studies are necessary. In this study, we carried out the backbone chemical shift assignment using a suite of heteronuclear triple resonance NMR experiments. We obtained the secondary structures of phospho-*Tt*IIB^{Mtl} based on the backbone dihedral angles derived from chemical shifts using TALOS+ program, which were consistent with the global fold of *Ec*IIB^{Mtl}.

* Correspondence to: **Jeong-Yong Suh,** Department of Agricultural Biotechnology, Seoul National University, Seoul 08826, Korea Tel: 82-2-880-4879; Fax: 82-2-877-4906; E-mail: jysuh@snu.ac.kr

Experimental Methods

Sample preparation- The gene *Tt*IIB^{Mtl} (385-477) was PCR-amplified from *Thermoanaerobacter Tengcongensis* genomic with the following primers : *Tt*IIB^{Mtl} forward (5' GTGCCACGCGGTTCTAAAATGGATACCCTG CCGAAACTC), and *Tt*IIB^{Mtl} reverse (3' GAGTTTCGGCAGGGTATCCATTTTAGAACC GCGTGGCAC). The PCR product was digested with *NcoI* (Thermo Fisher Scientific) and *XhoI* (Thermo Fisher Scientific) restriction enzyme and subcloned into the modified pET-32a vector with N-terminal 6xHis-Trx tag separated by a TEV cleavage site. The phosphoryl residue, Cys-395, was mutated to Ser using the QuickChange kit (Agilent Technologies), and the new construct sequence was verified by DNA sequencing. The plasmid were introduced into *Escherichia coli strain BL21star(DE3) (Invitrogen) cell*s for expression. Cells were grown in minimal medium supplemented by $^{15}NH_4Cl$ and $^{13}C_6$-glucose, induced with 1 mM isopropyl-D-thiogalactopyranoside at an A_{600} *of 0.7*, and harvested by centrifugation after overnight of induction. The cell pellet was resuspended in 50 ml (per liter of culture) of 20 mM Tris, pH 7.4, 200 mM NaCl and 1 mM phenylmethylsulfonyl fluoride. The suspension was lysed by three passages through Emulsiflex (Avestin, Canada) after homogenizing and centrifuged at 24,000*g* for 20 min at 4ºC. The supernatant fraction was filtered and loaded onto a HisTrap nickel-Sepharose column and the fusion protein was eluted with a 100-ml gradient of imidazole (10–500mM). The protein was then dialyzed against 50 mM Tris, pH 8.0, 4mM β-mercaptoethanol and digested with TEV protease. The cleaved 6xHis-Trx tag was removed by loading the digested proteins over a nickel-Sepharose column. Relevant fractions were purified by Superdex 75 gel filtration column (GE Healthcare) equilibrated with 20 mM Tris-HCl, pH 7.4, 200 mM NaCl and then on a monoS cation exchange column (8ml; GE Healthcare) with a 160-ml gradient of 1M NaCl. Phosphorylation of *Tt*IIB^{Mtl} was conducted as previous study.[10] Phosphorylated proteins were finally concentrated in 20 mM Tris, pH 7.4. NMR samples contained 1mM [U-$^{15}N/^{13}C$]-phospho-*Tt*IIB^{Mtl} (C395S) in 20mM Tris, pH 7.4 and 90% H_2O /10% D_2O.

NMR experiments and structure calculation and secondary structure prediction - NMR spectra were collected at 298K on Bruker AVANCE 700MHz spectrometers equipped with a *z*-shielded gradient triple resonance cryoprobe. Spectra were processed using the NMRPipe program[11] and analyzed using the PIPP/CAPP/STAPP program[12] and NMRView.[13] Sequential assignment of ^{13}C, ^{15}N-labeled phospho-*Tt*IIB^{Mtl} protein was using 2D ^{15}N-HSQC spectrum and 3D triple resonance through-bond scalar correlation experiments such as 3D HNCO, HNCACO, HNCA, HN(CO)CA, HNCACB, CBCA(CO)NH experiments[14,15] Overall secondary structure and the backbone dihedral torsion angles were predicted from TALOS+[16] based on combined H_N, ^{15}N, C_α, C_β and CO backbone chemical shifts.

Results and Discussion

Backbone assignment of phospho-*Tt*IIB^{Mtl} – Since the phosphoryl groups on cysteine were labile and slowly lost to buffer by acid-catalyzed dephosphorylation reactions, the active site Cys395 of *Tt*IIB^{Mtl} was mutated to serine which could be permanently phosphorylated as a stable form. *Tt*IIB^{Mtl}(C395S), consists of 92 amino acid residues with molecular weight of 10.6 kDa. We carried out a suite of heteronuclear triple resonance NMR spectroscopy. The ^1H, ^{15}N and ^{13}C assignment obtained for phospho-*Tt*IIB^{Mtl} (C395S) are listed in Table 1. Backbone assignments for amide resonances were obtained for 82 residues out of 89 residues (92%), excluding three proline residues. The backbone amide resonances with missing assignment are between F462 and V467 that corresponds to a flexible loop in phospho-*Ec*IIB^{Mtl} (C384S).[6] The amide resonances of the loop region were completely broadened out due to an exchange with the solvent

and conformational changes in the flexible loop. In comparison with amide peaks of the free *Tt*IIB^{Mtl}, the residues near the active site phosphorylated Ser395 showed large chemical shift perturbations. The assignments are annotated with residue types and numbers in Figure 1. In summary, 92% of C_α, 93% of C_β and 90% of CO were assigned and listed in Table 1.

Secondary structure of phospho-TtIIB^{Mtl} - Secondary structural information of phospho-*Tt*IIB^{Mtl} was calculated by using TALOS+ program[16] based on the ^1H_N, ^{15}N, Cα, Cβ and CO chemical shifts. The height of the bars indicates the probability of the secondary structure prediction (Fig. 2 upper panel). The secondary structure prediction showed that phospho-*Tt*IIB^{Mtl} (C395S) is comprised of four β strands and three α-helices. Residue L390~S395 (β1), F418~A426 (β2), V436~T439 (β3) and K455~V459 (β4) constitute the β strands, and S401~E415 (α1), E441~V450 (α2) and F462~L475 (α3) constitute the α-helices. Phospho-*Ec*IIB^{Mtl} is composed of central four beta strands flanked by three alpha helices. The results of backbone torsion angles (φ, ψ) are presented in Ramachandran plot (Figure 2 lower panel), 73 residues are in most favorable regions, and six residues are in allowed region, and three residues are in generously allowed regions. Clearly, the secondary structure prediction and torsion angle prediction data suggest that phospho-*Ec*IIB^{Mtl} and phospho-*Tt*IIB^{Mtl} (C395S) share a common backbone scaffold. Our results demonstrate that phospho-*Ec*IIB^{Mtl} and phospho-*Tt*IIB^{Mtl} exploit different strategy to accomplish an efficient binding to their partner IIA^{Mtl} proteins. Small differences at the binding interface as well as variable dynamic nature are likely responsible for the disparate binding properties.

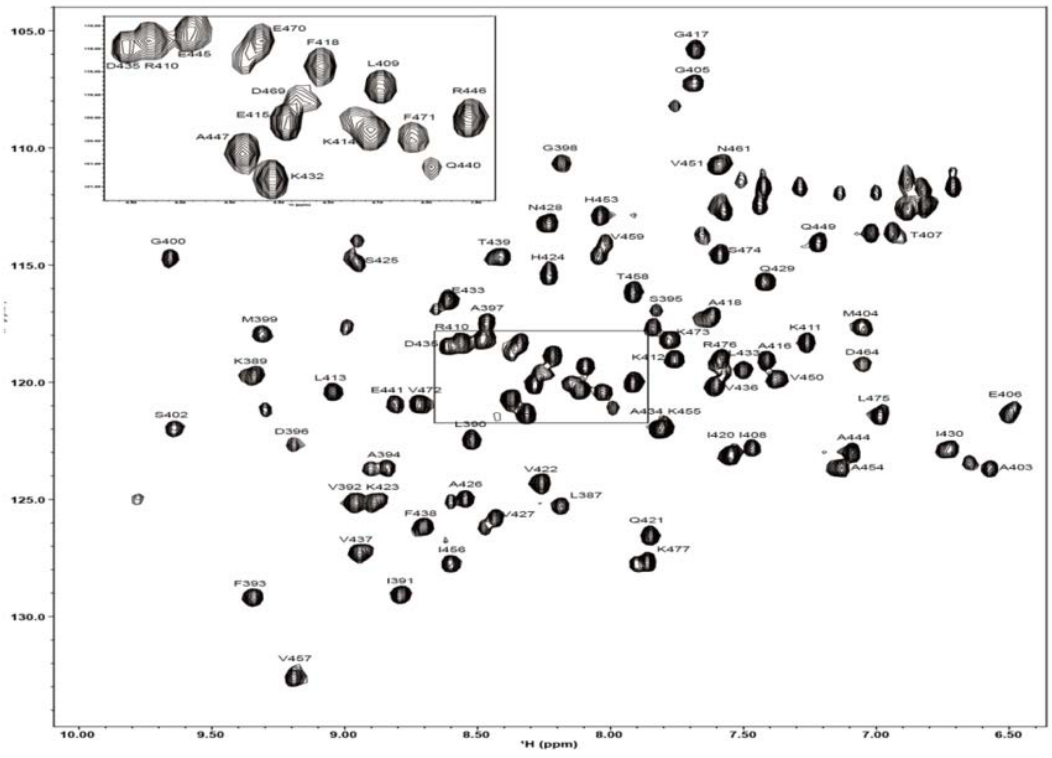

Figure 1. ^1H– ^{15}N HSQC spectra of $^{13}C/^{15}N$-labelled phospho-*Tt*IIB^{Mtl} in 20mM TrisHCl pH 7.4, 298K. The backbone amide cross peaks are annotated by residue names and numbers. An expansion of the boxed region is provided in the upper left corner.

Table 1. Backbone HN, N, C_α, C_β, CO chemical shifts of phospho-*Tt*IIB^{mtl} (unit:ppm)

Residue	HN	N	CA	CB	CO	Residue	HN	N	CA	CB	CO
386 THR	7.835	112.5	60.8	70.3	174.29	425 SER	9.005	114.99	58.14	67.58	174.59
387 LEU	8.21	125.21	53.25	41.95	175.09	426 ALA	8.579	124.94	52.12	19.02	177.02
388 PRO			62.83	32.76		427 VAL	8.504	126.2	65.62	31.59	177.62
389 LYS	9.405	119.8	57	33.78	173.92	428 ASN	8.278	113.23	54.5	37.61	175.8
390 LEU	8.573	122.48	55.49	43.13	174.25	429 GLN	7.475	115.79	63.75	37.62	175.88
391 ILE	8.813	129.04	59.57	40.17	173.22	430 ILE	6.763	122.86	60.82	39.55	
392 VAL	9.003	125.23	59.55	35.64	174.64	431 PRO			62.69	32.03	177.02
393 PHE	9.383	129.24	57.1	42.1	177.09	432 LYS	8.339	121.39	58.37	32.32	173.7
394 ALA	8.894	123.76	50.25	22.94	172.78	433 GLU	8.667	116.42	57.09	28.56	174.34
395 SER	7.879	117.78	55.88	68.37	176.73	434 ALA	7.852	122.1	53.97	19.35	175.43
396 ASP	9.227	122.68	58.77	41.78	178.63	435 ASP	8.654	118.46	55.46	43.88	172.65
397 ALA	8.486	117.42	52.19	20.01	174.81	436 VAL	7.651	120.21	60.2	36.85	178.47
398 GLY	8.217	110.66	46.59		176.52	437 VAL	8.991	127.37	59	35.36	178.21
399 MET	9.357	118.01	54.59	34.89	175.77	438 PHE	8.755	126.24	55.81	41.8	176.43
400 GLY	9.72	114.78	46.25		175.52	439 THR	8.493	114.76	60.41	70.39	179.28
401 SER	9.425	126.84	62.03	63.04	176.01	440 GLN	8.028	121.23	55.6	29.88	179.01
402 SER	9.718	122.09	61.24	62.38	179.66	441 GLU	8.724	120.93	60.5	29.91	179.02
403 ALA	6.701	123.49	53.8	17.26	178.8	442 ASN				36.79	175.55
404 MET	7.106	117.71	57.55	31.58	173.1	443 LEU	7.553	119.51	54.19	43.28	177.94
405 GLY	7.733	107.26	47.91		176.95	444 ALA	7.133	123.11	56.21	18.88	179.03
406 GLU	6.541	121.41	58.46	28.68	176.47	445 GLU	8.517	118.09	59.59	28.97	177.95
407 THR	7.06	113.68	66.29	68.77	178.43	446 ARG	7.922	119.93	58.64	30.05	176.99
408 ILE	7.515	122.85	64.96	38.1	181.37	447 ALA	8.407	120.81	55.38	17.83	173.9
409 ARG	8.135	119.42	57.86	40.18	178.46	448ALA	7.671	117.32	53.95	18.44	175.95
410 ARG	8.614	118.29	60.83	29.99	178.77	449 GLN	7.257	114.02	57.51	28.6	177.12
411 LYS	7.3	118.37	59.9	32.39	178.78	450 VAL	7.398	119.83	65.53	32.56	174.46
412 LYS	7.804	119.05	59.66	33.6	181.46	451 VAL	7.64	110.84	57.34	32.68	175.76
413 LEU	9.09	120.38	58.36	41.34	177.52	452 PRO			64.75	32.14	177.08
414 LYS	8.148	120.36	59.37	31.93	176.43	453 HIS	8.053	112.87	55.65	30.7	174.81
415 GLU	8.321	120.13	59.04	29.42	174.19	454 ALA	7.172	123.78	51.79	19.34	178.53
416 ALA	7.466	119.18	52	19.97	174.94	455 LYS	7.834	121.89	55.71	33.21	177.94
417 GLY	7.723	105.79	45.52		174.86	456 ILE	8.63	127.78	58.73	36.39	178.31
418 PHE	8.264	118.94	57.14	42.05	174.14	457 VAL	9.231	132.57	61.43	32.21	174.32
419 ASP	9.143	124.47	53.46	41.41	175.14	458 THR	7.948	116.14	59.85	69.81	177
420 ILE	7.544	123.15	60.45	42.52	176.12	459 VAL	8.091	114.54	58.33	34.57	174.75
421 GLN	7.912	126.58	57.12	29.77	173.03	460 LYS	9.077	122.17	58.16	32.32	177.21
422 VAL	8.26	124.24	59.91	34.33	182.42	461 ASN	7.396	112.55	52.24	40.77	
423 LYS	8.935	125.19	55.03	38.21	174.47	462 PHE					
424 HIS	8.256	115.12	63.14	30.91	176.06	463 LEU					

464 ASP						471 PHE	8.313	121.36	62.25	39.24	176.26
465 ASN						472 VAL	8.756	120.92	67.3	31.45	180.64
466 THR						473 LYS	7.825	118.26	59.37	32.44	177.87
467 VAL						474 SER	7.632	114.57	60.55	63.31	179.67
468 TYR	6.783	119.12	58.77	37.63	176.02	475 LEU	7.033	121.48	55.29	41.86	179.23
469 ILE	8.306	119.74	57.8	40.13	174.8	476 ARG	7.622	119.06	55.77	31.45	174.02
470 GLU	8.589	118.38	60.84	29.84	181.45	477 LYS	7.893	127.72	58.02	33.71	

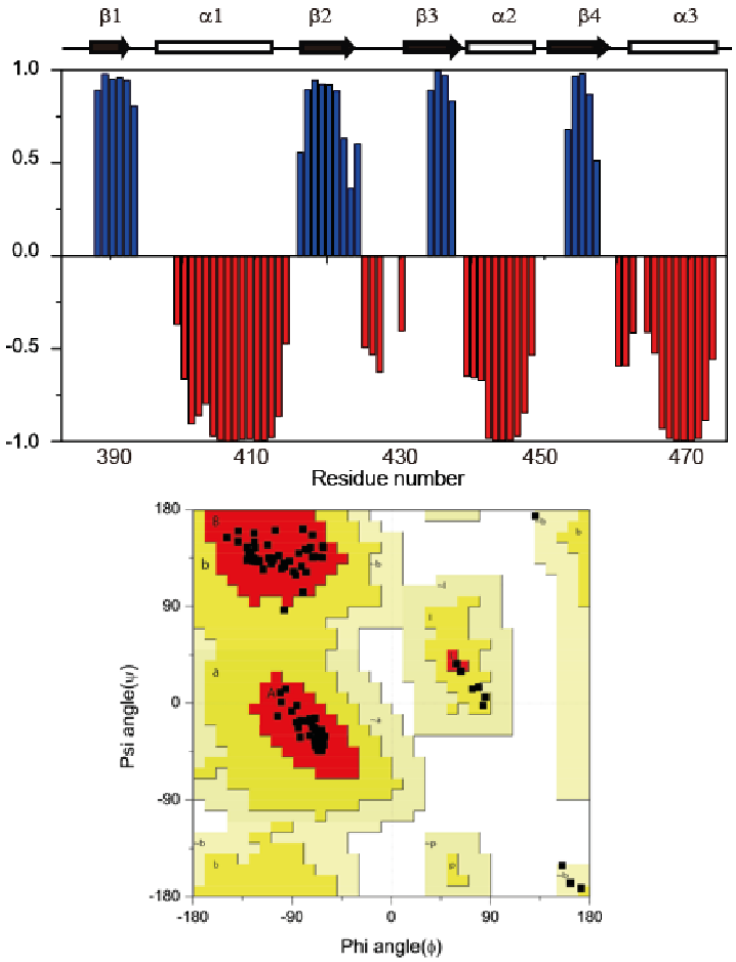

Figure 2. Predicted secondary structure (upper panel) and the backbone derived Ramachandran plot of phospho-*Tt*IIB^{Mtl} (lower panel). Predicted secondary structure (blue positive bar, beta-sheet; red negative bar, helix) for all residues are shown in the lower panel. The height of the bars reflects the probability of the neural network secondary structure prediction, and schematic representations of secondary structure are displayed above the prediction scores. (upper panel). Backbone torsion angles (ϕ, ψ) were predicted using TALOS+[16] with backbone chemical shifts and plotted upon the Ramachandran plot (lower panel)

Acknowledgements

This work was supported by Cooperative Research Program for Agriculture Science & Technology

Development, Rural Development Administration (PJ011112016). The authors thank the high field NMR facility at the Korea Basic Science Institute and the National Center for Inter-university Research Facilities.

References

1. P. W. Postma, J. W. Lengeler, and G. R. Jacobson, *Microbiol. Rev.* **57**, 543 (1993)
2. C. Siebold, K. Flukiger, R. Beutler, and B. Erni, *FEBS Lett.* **504**, 104 (2001)
3. J. Deutscher, C. Francke, and P. W. Postma, *Microbiol. Mol. Biol. Rev.* **70**, 939 (2006)
4. Q. Bao,Y. Tian, W. Li, Z. Xu, Z. Xuan, S. Hu, W. Dong, J. Yang, Y. Chen, Y. Xue, Y. Xu, X. Lai, L. Huang, X. Dong, Y. Ma, L. Ling, H. Tan, R. Chen, J. Wang, J. Yu, and H. Yang, *Genome Res.* **12**, 689 (2002)
5. P.M. Legler, M.Cai, A. Peterkofsky, and G. M. Clore, *J. Biol. Chem.* **279**, 39115 (2004)
6. Suh, C. Tang, M. Cai, and G. M. Clore, *J. Mol. Biol.* **353**, 1129 (2005)
7. J. Y. Suh, M. Cai, and G. M. Clore, *J. Biol. Chem.* **283**, 18980 (2008)
8. J. Y. Suh, J. Iwahara, and G. M. Clore, *Proc. Natl. Acad. Sci. U.S.A.* **104**, 3153 (2007)
9. V. P. R. Chichili, V. Kumar, and J. Sivaraman, *Protein Sci.* **22**, 153 (2013)
10. K. O. Lee, E. H. Kim, G. Kim, J. Y. Jung, S. Katayama, S. Nakamura, and J. Y. Suh, *Protein Sci*. **25**, 1803 (2016)
11. F. Delaglio, S. Grzesiek, G. W. Vuister, G. Zhu , J. Pfeifer, and A. Bax, *J. Biomol. NMR* **6**, 277 (1995)
12. D. S. Garrett, R. Powers, A. M. Gronenborn, and G. M. Clore, *J. Magn. Reson.* **95**, 214 (1991)
13. B. A. Johnson, and R. A. Blevins, *J. Biomol. NMR* **4**, 603 (1994)
14. M. D. Seo, S. J. Park, S. H. Seok, J. H. Kim, M. J. Cha, and B. J. Lee, *J. Kor. Magn. Reson. Soc.* **16**, 91 (2012)
15. K. O. Lee, and J. Y. Suh, *J. Kor. Magn. Reson. Soc.* **19**, 42 (2015)
16. Y. Shen, F. Delaglio, G. Cornilescu, and A. Bax , *J. Biomol. NMR* **44**, 213 (2009)